


# Cell immaturity and white/beige adipocyte potential of primary human adipose-derived stromal cells are restrained by culture-medium TGFβ1

Hélène Leménager<sup>1</sup>  | Loïc M. A. Fiévet<sup>1</sup> | Fabien Guilloton<sup>1</sup> | Abderrahim Naji<sup>2</sup> | Jean-Gérard Descamps<sup>1</sup> | Benoît Chaput<sup>3</sup> | Narufumi Suganuma<sup>2</sup> | Jean-Christophe Pagès<sup>1</sup> | Luc Sensebé<sup>1</sup> | Audrey Carrière<sup>1</sup> | Louis Casteilla<sup>1</sup> | Frédéric Deschaseaux<sup>1</sup>

<sup>1</sup>STROMALab, Etablissement Français du Sang-Occitanie (EFS), Inserm 1031, University of Toulouse, ERL5311 CNRS, National Veterinary School of Toulouse (ENVT), Toulouse, France

<sup>2</sup>Department of Environmental Medicine, Cooperative Medicine Unit, Research and Education Faculty, Medicine Science Cluster, Kochi Medical School (KMS), Kochi University, Nankoku City, Japan

<sup>3</sup>Department of Plastic, Reconstructive and Aesthetic Surgery, Rangueil University Hospital, Toulouse, France

## Correspondence

Louis Casteilla, PhD, STROMALab—Bâtiment INCERE, 4 bis avenue Hubert Curien 31100 Toulouse.  
Email: louis.casteilla@inserm.fr

Frédéric Deschaseaux, PhD, STROMALab—Bâtiment INCERE, 4 bis avenue Hubert Curien 31100 Toulouse.  
Email: frederic.deschaseaux@efs.sante.fr

Hélène Leménager, PhD, STROMALab—Bâtiment INCERE, 4 bis avenue Hubert Curien 31100 Toulouse.  
Email: helene.lemenager@inserm.fr

## Funding information

Etablissement Français du Sang Scientific Council, Grant/Award Number: APR 2014; Japanese Society for the Promotion of Science (JSPS), Grant/Award Number: 17K15729; French Research and Educational Ministry at Paul Sabatier University

## Abstract

Human adipose-derived stem/stromal cells (hASCs) can differentiate into specialized cell types and thereby contribute to tissue regeneration. As such, hASCs have drawn increasing attention in cell therapy and regenerative medicine, not to mention the ease to isolate them from donors. Culture conditions are critical for expanding hASCs while maintaining optimal therapeutic capabilities. Here, we identified a role for transforming growth factor β1 (TGFβ1) in culture medium in influencing the fate of hASCs during in vitro cell expansion. Human ASCs obtained after expansion in standard culture medium (Standard-hASCs) and in endothelial cell growth medium 2 (EGM2-hASCs) were characterized by high-throughput transcriptional studies, gene set enrichment analysis and functional properties. EGM2-hASCs exhibited enhanced multipotency capabilities and an immature phenotype compared with Standard-hASCs. Moreover, the adipogenic potential of EGM2-hASCs was enhanced, including toward beige adipogenesis, compared with Standard-hASCs. In these conditions, TGFβ1 acts as a critical factor affecting the immaturity and multipotency of Standard-hASCs, as suggested by small mother of decapentaplegic homolog 3 (SMAD3) nuclear localization and phosphorylation in Standard-hASCs vs EGM2-hASCs. Finally, the typical priming of Standard-hASCs into osteoblast, chondroblast, and vascular smooth muscle cell (VSMC) lineages was counteracted by pharmacological inhibition of the TGFβ1 receptor, which allowed retention of SMAD3 into the cytoplasm and a decrease in expression of osteoblast and VSMC lineage markers. Overall, the TGFβ1 pathway appears critical in influencing the commitment of hASCs toward osteoblast, chondroblast, and VSMC lineages, thus reducing their adipogenic potential. These effects can be counteracted by using EGM2 culture medium or chemical inhibition of the TGFβ1 pathway.

**Abbreviations:** ASCs, adipose-derived stem/stromal cells; BM-MSCs, bone marrow mesenchymal stem/stromal cells; BMP, bone morphogenetic protein; CFU-f, colony-forming unit fibroblast; EGM2, endothelial cell growth medium 2; FBS, fetal bovine serum; GO, Gene Ontology; GSEA, gene set enrichment analysis; hrTGFβ1, human recombinant transforming growth factor-beta 1; MEM, minimum essential media; MSCs, mesenchymal stem/stromal cells; PCA, principal component analysis; SMAD, small mother of decapentaplegic homolog; SVF, stromal vascular fraction; TGFβ1R, transforming growth beta 1 receptor; TGFβR1, transforming growth beta receptor type 1; UCP1, uncoupling protein 1; VSMCs, vascular smooth muscle cells.

**KEYWORDS**

adipose-derived stromal cells, beige adipocyte, chondroblast, mesenchymal stem/stromal cells, osteoblast, transforming growth factor-beta 1, vascular smooth muscle cell, white adipocyte

**1 | INTRODUCTION**

Mesenchymal stem/stromal cells (MSCs) are multipotent cells that can differentiate into multiple cell types and contribute to tissue regeneration.<sup>1</sup> Hence, MSCs hold important interest in cell therapy and regenerative medicine.<sup>2</sup> MSCs were first identified in bone marrow (BM-MSCs), which remains their main biological source in research and cell therapy.<sup>3</sup> Alternatively, adipose-derived stromal cells (ASCs) are MSCs accessible from adipose tissue, by simple procedures and at high cell yield.<sup>4</sup>

Subcutaneous adipose tissue contains at least 2 types of adipocytes: mostly white adipocytes and beige adipocytes.<sup>5,6</sup> White adipocytes store and release lipids, whereas beige adipocytes express the uncoupling protein 1 (UCP1) promoting lipid and glucose oxidization. Recently, beige adipocytes have drawn interest in medicine because of their ability to prevent metabolic diseases, such as obesity and type 2 diabetes in animal models.<sup>7,8</sup> Therefore, the differentiation of hASCs and/or the conversion of white adipocytes into beige adipocytes are of clinical interest.<sup>7,9</sup> By affecting ASC functionality but lacking standardization, hASC culture represents a major bottleneck and deserves specific attention.<sup>3</sup> For expanding hASCs, we used the endothelial cell growth medium 2 (EGM2), designed for culturing endothelial and perivascular cells, a physiological location common to hASCs.<sup>10-13</sup> Of note, the most used condition for hASCs expansion, standard medium, differs from EGM2 notably by a content of 10% of fetal bovine serum (FBS), compared with 2% FBS for EGM2.

Transforming growth factor β1 (TGFβ1) is one of the components of FBS.<sup>14</sup> It belongs to the TGFβ superfamily with bone morphogenetic proteins (BMPs), activins, and others.<sup>15</sup> TGFβ1 is secreted as a latent protein complex and stored in the extracellular matrix (ECM). Following tensile forces,<sup>16</sup> pH changes,<sup>17</sup> or plasmin's serine protease activity,<sup>18</sup> the noncovalent binding between the pro-TGFβ1 and the latency-associated peptide is disrupted and TGFβ1 is activated.<sup>19</sup> TGFβ1 binds to cell surface receptors consisting of type I (TGFβRI) and type II (TGFβRII) receptor serine/threonine kinases that propagate signaling via phosphorylation of effector proteins, such as small mother of decapentaplegic homolog (SMAD), notably SMAD3. SMAD3 is phosphorylated by TGFβRI and heterodimerizes with SMAD4 to form an active SMAD complex.<sup>20</sup> Activated SMAD complex translocates into the nucleus, thus enabling transcription of genes involved in cell differentiation, growth, and proliferation.

Here, we observed that hASCs expanded in vitro in a standard medium (Standard-hASCs) were essentially primed into osteoblast, chondroblast, and vascular smooth muscle cell (VSMC) lineages. We also showed that EGM2-hASCs retained features of cell immaturity and exhibited an enhanced adipogenic potential, with beige adipocyte

**Significance statement**

Human adipose-derived stem/stromal cells (hASCs) are typically expanded in serum-containing media. The current study shows that the transforming growth factor β1 (TGFβ1) contained in serum induces the commitment of hASCs toward osteoblast, chondroblast, and vascular smooth muscle cell lineages. This commitment impedes the immaturity of hASCs and their adipogenic potential during in vitro cell expansion, including toward the beige adipocyte. Standard culture medium affects the cell multipotency of hASCs, a crucial feature to consider when improving methods of hASC expansion to obtain clinical grade hASCs. The study details the effect of TGFβ1 on hASC culture and propose alternative culture methods to expand hASCs with optimal therapeutic interests.

potential. Furthermore, high-throughput transcriptomic, gene set enrichment analysis (GSEA), and functional experiments confirmed the immaturity of EGM2-hASCs and allowed us to identify TGFβ1 as a critical factor affecting the hASC fate during in vitro cell expansion. Accordingly, inhibition of TGFβ1 receptor (TGFβ1R) in Standard-hASCs was sufficient to restore the immaturity of hASCs, with strong beige adipogenic potential.

Our results highlight the need to consider the effect of TGFβ1 on hASCs during in vitro cell expansion in standard medium culture conditions. These findings should prompt the alternative use of EGM2 to expand hASCs, for optimal therapeutic potential in regenerative medicine and metabolic disorders.

**2 | MATERIALS AND METHODS****2.1 | Isolation of hASCs, expansion media, and cell culture**

Abdominal dermolipectomia tissues were obtained from 46 women after reconstructive surgery (mean body mass index  $26.9 \pm 0.4$  kg/m<sup>2</sup> [range 18.7-32.7 kg/m<sup>2</sup>]; mean age  $41.4 \pm 1.7$  years [range 18-66 years]). Experimental protocols were approved by an ethics committee (No: DC-2015-23-49), and informed consent was obtained from all participants. Human adipose tissue was dissected with scissors and underwent

enzymatic digestion with 13.6 U/mL collagenase NB4 (Serva Electrophoresis, Heidelberg, Germany) at 37°C under agitation for 45 minutes in minimum essential media (MEM) containing Glutamax (Life Technologies, Carlsbad, California) supplemented with 1% penicillin/streptomycin (Life Technologies). Homogenates were 100- $\mu$ m-filtered (Sterifip; Millipore, Burlington, Massachusetts), and the stromal vascular fraction (SVF) was isolated by centrifugation for 10 minutes at 500g. The SVF was plated at 4000 cells/cm<sup>2</sup> in a standard medium—MEM Glutamax 1% penicillin/streptomycin, 10% FBS (Life Technologies), and 1 ng/mL fibroblast growth factor 2 (Reliatech GmbH, Wolfenbüttel, Germany)—or EGM2 with 2% FBS and defined supplements (reference C-22011; PromoCell, Heidelberg, Germany; <https://www.promocell.com/product/endothelial-cell-growth-medium-2/>). After 7 days, hASCs were analyzed or treated with 10 ng/mL TGF $\beta$ 1 (Miltenyi Biotech, Bergisch Gladbach, Germany) or 1  $\mu$ M SB431542 or SB505124 ALK5 TGF $\beta$ 1R inhibitors (Tocris Bioscience, Bristol, UK). All experiments were performed with hASCs at passage 0 unless stated otherwise.

## 2.2 | Multipotential assays

Osteogenesis was induced by 50  $\mu$ M ascorbic acid (Sigma-Aldrich, Saint-Louis, Missouri) and 10 mM  $\beta$ -glycerophosphate (Sigma) in  $\alpha$ MEM (Life Technologies), 2% FBS and 1% L-glutamine (Life Technologies). At day 11, cultures were fixed with 4% formaldehyde (Sigma) and stained with Alizarin red S (Sigma), then dissolved in 10% acetic acid. Absorbance was read at 405 nm by spectrophotometry (Varioskan, Thermo Fisher; Waltham, Massachusetts).

Commitment toward chondrogenesis was induced by 3 weeks of 2D-culture in high-glucose DMEM (Life Technologies) complemented with 1 mM sodium pyruvate, 0.1  $\mu$ M dexamethasone, 0.17 mM ascorbic-2-phosphate acid, 0.35 mM L-proline, 1% insulin transferrin selenium+1 (all Sigma), and 10 ng/mL TGF $\beta$ 3 (R&D Systems; Minneapolis, Minnesota). Cells were fixed with 4% paraformaldehyde and stained with Alcian blue (Sigma).

Adipogenesis was induced by culture for 11 days in MEM containing Glutamax supplemented with 10% FBS, 1  $\mu$ M dexamethasone, 5  $\mu$ g/mL insulin, 1  $\mu$ M rosiglitazone, and 60  $\mu$ M indomethacin (all Sigma) or MEM supplemented with 2% FBS, 1  $\mu$ M dexamethasone, 1  $\mu$ g/mL insulin, and 0.5 mM isobutylmethylxanthine (Sigma). In some experiments, conversion of white to beige adipocytes was induced by overnight treatment with 2  $\mu$ M forskolin (Sigma). Adipogenesis was assessed in cells fixed in glutaraldehyde 3% and stained for neutral lipids with Oil-red O (Sigma), then dissolved in 60% isopropanol. Absorbance at 510 nm was read by using Varioskan spectrophotometry (ThermoFisher).

## 2.3 | Western blot analysis

Cells were lysed in RIPA buffer (Biotech; Markham, ON, Canada) supplemented with a complete mini-EDTA-free protease inhibitors cocktail (Roche, Bâle, Suisse) and phosphatase inhibitors cocktail (Sigma). Proteins were quantified with MicroBCA (Thermo Fisher). Electrophoresis

was performed in Mini Protean TGX Gel 12% SDS (Biorad, Hercules, California), bathed in tris-glycine-SDS buffer (Biorad). Proteins were transferred to polyvinylidene difluoride membrane (Biorad) in tris-glycine buffer (Biorad). Membranes were incubated in PBS 0.1% Tween-20 (Biorad), 5% nonfat dry milk and primary antibodies for OCT4 (ab19857, Abcam, Cambridge, UK), SOX2 (ab97959, Abcam), NANOG (AF1997, R&D),  $\beta$ -Actin (A5441, Sigma), PPAR $\gamma$  (2443S, Cell Signaling Technology [CST], Danvers, Massachusetts), Calponin1 (MAB9569 Abnova, Taiwan), FABP4 (AF1443, R&D), GAPDH (ab8245, Abcam), p-SMAD3 (9520S, CST), or SMAD3 (9513S, CST). Proteins were revealed with horseradish peroxidase-conjugated goat anti-rabbit or anti-mouse IgG (1 706 515 and 1 706 516, Biorad, respectively) or rabbit anti-goat IgG (81-1620, Thermo Fisher) and ECL detection (Biorad). ImageJ (National Institutes of Health; Bethesda, Maryland) was used for protein semi-quantification.

## 2.4 | Quantitative RT-PCR

Cells were lysed in RLT (Qiagen, Hilden, Germany). RNA was extracted by using the RNeasy Plus Mini kit (Qiagen) and reverse-transcribed by using the High-Capacity cDNA Reverse Transcription kit (Applied Biosystems, Foster City, California) following the manufacturer's instructions for 10 minutes at 25°C, 120 minutes at 37°C, and 5 minutes at 85°C. qPCR involved using 300 nM primers listed in Table S1 and FAST SYBR Green Reagent (Applied Biosystems) with a StepOne device (Applied Biosystems). Data were analyzed with StepOne software and normalized to the housekeeping gene expression and the standard control sample unless stated otherwise. Fold change in mRNA content was determined according to the  $2^{-\Delta\Delta C_t}$  method. Relative comparison was calculated as  $\Delta\Delta C_t(x) = \Delta C_t(x) - \Delta C_t(\text{Ctrl})$  with  $\Delta C_t(x \text{ or Ctrl}) = C_t(x \text{ or Ctrl}) - C_t(\text{housekeeping genes})$  with  $x$  = the sample mRNA.

## 2.5 | Flow cytometry

Standard-hASCs or EGM2-hASCs were trypsinized (Life Technologies) and blocked in 0.1% human serum albumin (LFB Biomedicaments; Courtaboeuf, France). Cells were stained with CD90 (555596), CD73 (550257), CD13 (555394), CD45 (555483), CD31 (555446), and CD34 (555822), all conjugated with phycoerythrine (BD Biosciences, Franklin Lakes, New Jersey), and staining was analyzed with an ADP Cyan flow cytometer (Beckman Coulter; Brea, California). Data were analyzed with Kaluza v1.2 (Beckman Coulter). Dead cells were excluded by DAPI staining (Sigma).

## 2.6 | Colony-forming unit-fibroblast analysis

SVF was serially diluted from 128 to 1 cells per well in 96-well plates. After 10 days, cells were fixed in absolute methanol for 5 minutes and stained in 10% Giemsa (Sigma) for 10 minutes. Colony-formation assay involved using Poisson distribution statistics by determining the

number of wells with no clonogenic growth at day 10. Aggregates of >10 cells were scored as colony-forming unit-fibroblasts (CFU-f)-derived colonies as previously described.<sup>21</sup>

## 2.7 | Affymetrix assay

cDNA synthesis and amplification were performed on high-quality mRNA (RQI >9.8) by using the Ovation PicoSL WTA-System V2 protocol (NuGEN, Redwood City, California). An amount of 25 ng mRNA was reverse-transcribed in primer mix containing poly-T and random sequences for whole-transcriptome coverage, followed by a second-strand cDNA synthesis with Ribo-SPIA technology (NuGEN). An amount of 2.5 μg SPIA cDNA was fragmented and biotinylated in Encore Biotin Module (NuGEN) and hybridized (48°C, 20 hours) with the Affymetrix HuGene1.1STArray Strip Kit (Affymetrix, Santa Clara, California). Arrays were scanned by using the Affymetrix GeneAtlas imaging station. Scanned images (DAT files) were analyzed with Affymetrix GeneChip Command Console software. Data were imported into Partek Genomics Suite software (Partek, Inc., Missouri). The Robust Multichip Analysis algorithm was used for generating signal values. Principal component analysis (PCA) was used for global 3D unsupervised analysis. Partek Genomics Suite software was used for generating specific gene expression signatures (fold change >2), and for Gene Ontology (GO) enrichment analysis. Ingenuity Pathway Analysis (Ingenuity Systems, www.ingenuity.com) was used for gene networks and canonical pathways analysis.

## 2.8 | Gene set enrichment analysis

We used GSEA software from Broad Institute (<http://software.broadinstitute.org/gsea/index.jsp>).<sup>22,23</sup> Gene signatures and raw data are accessible in the Gene Expression Omnibus repository platform (GSE136778). Analyses of molecular pathways involved the Database for Annotation, Visualization, and Integrated Discovery.<sup>24,25</sup>

## 2.9 | Enzyme linked immunosorbent assay

Sandwich enzyme linked immunosorbent assay was performed on medium or supernatant of cell cultures for bovine or human TGFβ1 according to the manufacturer's instructions (Boster Biological Technology; Pleasanton, California).

## 2.10 | Immunofluorescence assay

Cells were fixed in 3.7% paraformaldehyde (Sigma), permeabilized with 0.2% Triton X-100 (Sigma), and incubated overnight at 4°C with an anti-SMAD3 primary antibody (9513S, CST). Staining was revealed by using a donkey Alexa Fluor 488-nm anti-rabbit antibody (A21206, Molecular Probes; Eugene, Oregon) along with DAPI staining

(1:10000; D9542, Sigma). Images of cells were acquired on an LSM 780 confocal microscope (Zeiss, Oberkochen, Germany) or epifluorescence biphotonic microscope (Leica Biosystems, Nanterre, France). Fluorescence was analyzed with ImageJ (National Institutes of Health).

## 2.11 | Statistical analysis

GraphPad Prism 5 (GraphPad Software; San Diego, California) was used for statistical analysis and graph design. Data are expressed as mean ± SEM. Wilcoxon or Mann-Whitney tests were used for statistical analysis, with  $P < .05$  considered statistically significant, and statistical significance was shown with \* $P < .05$ , \*\* $P < .01$ , and \*\*\* $P < .001$ .

## 3 | RESULTS

### 3.1 | EGM2-hASCs exhibit cell immaturity features

In culture, both Standard-hASCs and EGM2-hASCs displayed similar fibroblast-like morphology (Figure S1a) and expressed CD90, CD73, and CD13 but not CD45 or CD31 (Figure S1b). EGM2 culture conditions led to fivefold less CFU-f from SVF compared with standard conditions (Figure S1c), but we obtained twice more adherent cells with EGM2 vs standard conditions after 7 days of cell expansion (Figure S1d). These results suggest that although both Standard-hASCs and EGM2-hASCs had a close phenotype, EGM2-hASCs showed an enhanced proliferation ability compared with Standard-hASCs. Also, under appropriate stimulations, EGM2-hASCs could differentiate into osteoblasts and chondroblasts as efficiently as Standard-hASCs (Figures 1A and S1e). Remarkably, EGM2-hASCs exhibited enhanced ability to differentiate into adipocytes compared with Standard-hASCs (Figures 1A and S1e).

To compare the cell immaturity of Standard-hASCs and EGM2-hASCs, we studied the expression of stemness markers. Notably, sex-determining region Y-box (SOX) 2, octamer-binding transcription factor (OCT) 4, and NANOG were found essential to maintain cell immaturity via cooperative interactions.<sup>26</sup> We found increased protein content of SOX2, OCT4, and NANOG, by at least twofold in EGM2-hASCs compared with Standard-hASCs (Figure 1B). Furthermore, EGM2-hASCs exhibited reduced priming toward the osteoblast lineage, as shown by decreased mRNA content of *distal-less homeobox 5* (*DLX5*), *collagen type 1α1* (*COL1α1*), and *alkaline phosphatase liver* (*ALPL*), compared with Standard-hASCs (Figure 1C). Moreover, levels of chondroblast lineage-associated mRNAs such as *hyaluronan and proteoglycan link protein 1* (*HAPLN*) and *SOX9* were greatly reduced in EGM2-hASCs compared with Standard-hASCs (Figure 1C). Similarly, levels of VSMC lineage-associated mRNAs, including *smooth muscle actin 2* (*ACTA2*) and *calponin 1* (*CNN1*), were decreased in EGM2-hASCs compared with Standard-hASCs (Figure 1C). In contrast, EGM2-hASCs exhibited increased levels of mRNAs associated with the adipocyte lineage, including *fatty acid-binding protein 4* (*FABP4*) and *lipoprotein lipase*



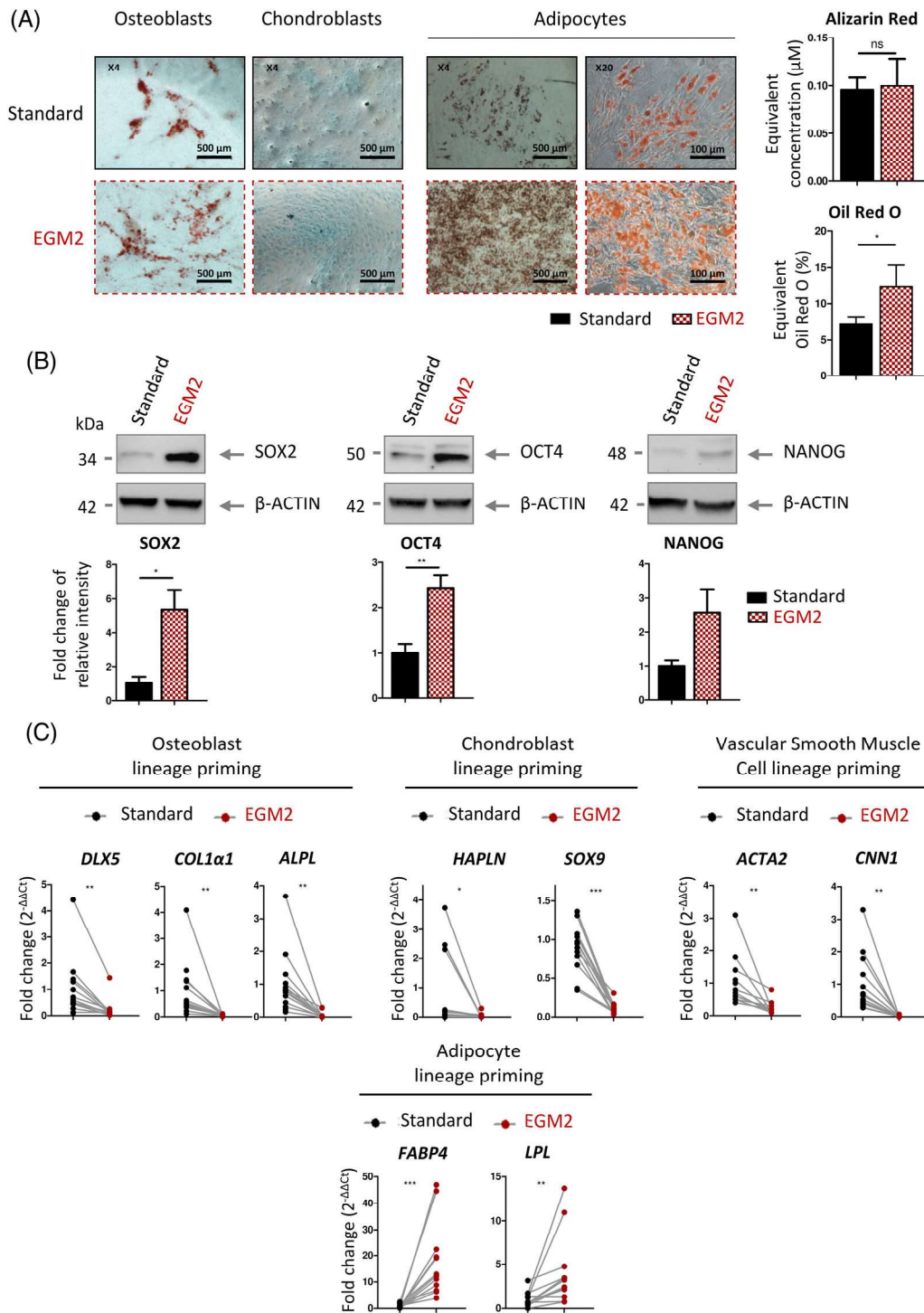


**FIGURE 1** Differentiation potential and immature state of EGM2-hASCs. A-C, Differentiation potential (A) and immature state (B-C) evaluation of hASCs expanded in MEM with 10% FBS (Standard; black) or EGM2 medium (EGM2; red). \*  $P < .05$ , \*\*  $P < .01$ , \*\*\*  $P < .001$ . A, Both types of hASCs were submitted to osteogenic, chondrogenic and adipogenic differentiation and were then analyzed for calcium deposition staining with Alizarin red (left panels), sulfated proteoglycan staining with Alcian blue (middle panels) and lipid staining with Oil-red O (right panels), respectively. Photonic microscopy. The calcium deposition and lipid content was quantified by chemical processes.  $n = 3$ , Wilcoxon test. Scale bar = 500  $\mu\text{m}$  or 100  $\mu\text{m}$ , magnification = 4 $\times$  or 20 $\times$  respectively. B, Western blot analysis of SOX2, OCT4, and NANOG proteins in both types of hASCs after expansion.  $\beta$ -ACTIN was a loading control. Data were quantified according to band intensity normalized to the corresponding  $\beta$ -ACTIN band and expressed as fold change relative to Standard condition.  $n = 4$ , Mann-Whitney test. C, RT-qPCR analysis of mRNA levels of characteristic markers for osteoblast (*DLX5*, *COL1 $\alpha$ 1*, and *ALPL*), chondroblast (*HAPLN* and *SOX9*), vascular smooth muscle cell (VSMC; *ACTA2* and *CNN1*) and adipocyte (*FABP4* and *LPL*) lineages in both types of hASCs after expansion. Data are expressed as fold change relative to both the housekeeping gene and Standard condition.  $n = 13$ , Wilcoxon test. EGM2, endothelial cell growth medium 2; FBS, fetal bovine serum; hASCs, human adipose-derived stem/stromal cells; MEM, minimum essential media

(LPL), compared with Standard-hASCs (Figure 1C). These findings suggest that EGM2-hASCs were more immature than Standard-hASCs.

### 3.2 | EGM2-hASCs exhibit enhanced adipogenic potential

We further analyzed the adipogenic potential of EGM2-hASCs and Standard-hASCs notably with rosiglitazone, an agonist of the master adipogenic regulator peroxisome proliferator-activated receptor  $\gamma$ 2 (PPAR $\gamma$ 2). We observed an enhanced adipogenic potential for EGM2-hASCs (Figure 2A,B). This was assessed by increased mRNA content of PPAR $\gamma$ 2 as well as FABP4, LPL, adiponectin (ADIPOQ) and CCAAT enhancer-binding protein  $\alpha$  (CEBP $\alpha$ ) (Figure 2A). Accordingly, we detected higher protein expression of PPAR $\gamma$ 2 in EGM2-hASCs than Standard-hASCs and especially after adipogenic differentiation (Figure 2B).

Taking into account that EGM2-hASCs were prone to adipogenic differentiation and considering that chronic treatment with rosiglitazone promoted also the beige adipocyte phenotype,<sup>27</sup> we evaluated the beige adipocyte potential of EGM2-hASCs and Standard-hASCs. Our results confirmed that adipocytes obtained from EGM2-hASCs overexpressed beige adipocyte mRNAs, including UCP1, cell death-inducing DFFA like effector A (CIDEA), and PPAR $\gamma$  coactivator 1 $\alpha$  (PGC1 $\alpha$ ) (Figure 2C). Subsequently, we used an alternative method to differentiate both EGM2-hASCs and Standard-hASCs into adipocytes, with a differentiation medium not containing rosiglitazone,<sup>7</sup> to avoid hASCs differentiation into beige adipocytes. Under those conditions, PPAR $\gamma$ 2 mRNA content increased about 10-fold in adipocytes derived from EGM2-hASCs compared with those derived from Standard-hASCs (Figure S2a). This finding confirmed that EGM2-hASCs were prone to differentiate to adipocytes to a greater extent than were Standard-hASCs. Moreover, UCP1 mRNA was virtually absent in adipocytes derived from both Standard-hASCs and EGM2-hASCs (Figure S2a), which confirmed that this alternative medium did not induce beige adipocytes. Subsequently, adipocytes were exposed overnight to the AMPc inducer forskolin in order to upregulate mRNAs associated with beige adipocytes. An increase in UCP1 mRNA content was measurable in adipocytes derived from both Standard-hASCs and EGM2-hASCs after forskolin stimulation (Figure S2a). Remarkably, UCP1 mRNA content in adipocytes derived from EGM2-hASCs was about ninefold higher than that observed in Standard-hASC-derived adipocytes. Moreover, CIDEA and PGC1 $\alpha$  mRNA levels were significantly increased by at least threefold in adipocytes derived from EGM2-hASCs, compared with standard counterparts (Figure S2a).

To evaluate the preservation of adipocyte differentiation capabilities during in vitro hASC expansion, we induced adipogenesis of Standard-hASCs and EGM2-hASCs at passages 0, 1, 2, 3, and 4. The mRNA levels of PPAR $\gamma$ 2, FABP4, LPL, and ADIPOQ in adipocytes from Standard-hASCs were greatly decreased as early as passage 2, whereas EGM2-hASCs retained intact adipogenic potential up to passage 4 (Figure 2D). Consistently, UCP1, CIDEA, and PGC1 $\alpha$  mRNA levels were maintained in EGM2-hASC-derived adipocytes (Figure 2E). By contrast, Standard-hASCs retained mRNAs levels associated with the osteoblast lineage, DLX5 and RUNX2, and also the chondroblast lineage, SOX9, and

VSMC lineage, including ACTA2, CNN1, and TGF $\beta$ 1. This was true after the adipogenic differentiation of Standard-hASCs compared with EGM2-hASCs (Figure S2b). Thus, EGM2-hASCs exhibited stronger white and beige adipogenic potential than Standard-hASCs.

### 3.3 | Transcriptomic analysis of Standard-hASCs confirms osteoblast, chondroblast, and VSMC priming

To validate our observations, we used a high-throughput transcriptomic analysis of Standard-hASCs and EGM2-hASCs. We observed that 62.4% of the genes in four-dimension PCA diverged in expression between Standard-hASCs and EGM2-hASCs (Figures 3A and S3A). Hence, among all genes analyzed, 981 showed significant differential expression by at least twofold in Standard-hASCs compared with EGM2-hASCs, with 535 genes upregulated in Standard-hASCs and 446 downregulated.

We used GSEA to analyze specific transcripts associated with osteoblast, chondroblast, adipocyte, and VSMC lineages. We found a clear adipocyte gene signature in EGM2-hASCs compared with Standard-hASCs (Figure S3b). Remarkably, PPAR $\gamma$ , perilipin (PLIN2), apolipoprotein D (APOD), PPAR $\alpha$ , fatty acid synthase (FASN), CEBP $\beta$ , FABP5, FABP4, and FABP3 were upregulated by  $\geq 1.5$ -fold in EGM2-hASCs vs Standard-hASCs (Figure S3c). Conversely, Standard-hASCs showed an anti-adipogenic gene signature (Figure S3d) that was notably underscored by the upregulation of Kruppel-like factor 2 (KLF2), KLF3, cyclin-dependant kinase inhibitor 1B (CDKN1B), nuclear receptor coactivator 2 (NCOA2), vitamin D receptor (VDR), and transcription factor 7 Like 2 (TCF7L2) (Figure S3e). Furthermore, we found upregulation of osteoblast (Figure S4a), chondroblast (Figure S4b), and VSMC (Figure S4c) lineage gene signatures in Standard-hASCs compared with EGM2-hASCs. Osteoblast-associated mRNAs, including COL12 $\alpha$ 1, podocan (PODN), COL1 $\alpha$ 1, ALPL, biglycan (BGN), and RUNX1, were upregulated by about threefold in Standard hASCs vs EGM2-hASCs (Figure S4d). Similarly, upregulated chondroblast-associated mRNAs included microfibril-associated protein 4 (MFAP4), dermatopontin (DPT), fibromodulin (FMOD), angiopoietin 1 (ANGPT1), cytochrome P450 family 1 subfamily B member 1 (CYP1B1), and ADAM metalloproteinase with thrombospondin type 1 motif 2 (ADAMTS2), with mRNA levels increased by at least twofold in Standard-hASCs compared with EGM2-hASCs (Figure S4e). Finally, VSMC-associated mRNAs upregulated in Standard-hASCs compared with EGM2-hASCs included CNN1, gap junction protein alpha 1 (GJA1), phosphodiesterase 3A (PDE3A), myosin 1C (MYO1C), tropomyosin 1 (TPM1), and endoglin (ENG) (Figure S4f). Hence, Standard-hASCs exhibited priming toward osteoblast, chondroblast, and VSMC lineages compared with EGM2-hASCs showing distinctive priming toward an adipocyte lineage.

### 3.4 | TGFβ1 pathway is involved in influencing the fate of Standard hASCs

To identify the molecular pathway regulating the biological properties of Standard-hASCs and EGM2-hASCs, we performed GO pathway

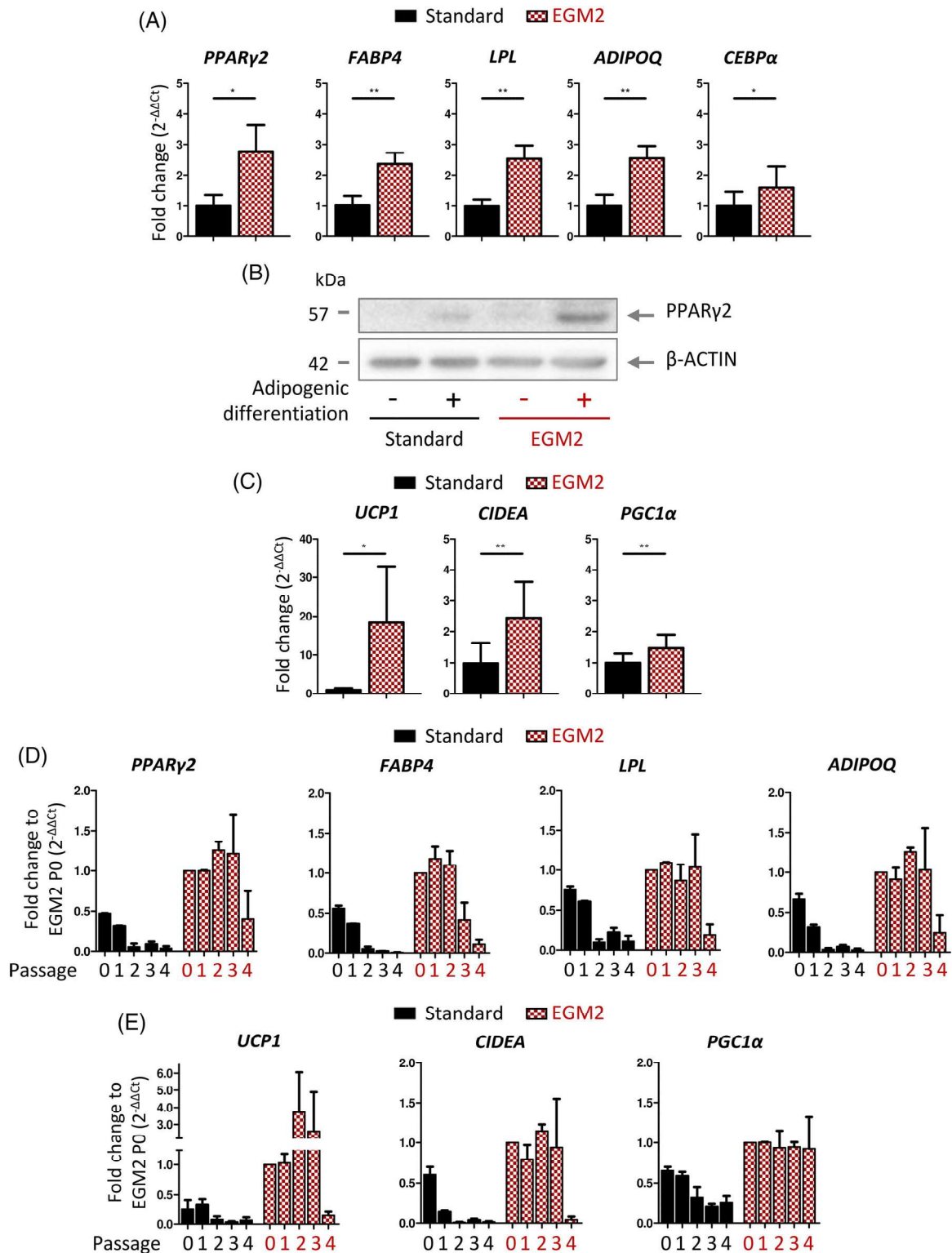


**FIGURE 2** White/beige adipogenic potential of Standard- and EGM2-hASCs. A-E, Standard-hASCs (black) and EGM2-hASCs (red) from passage 0 (A-C) to P4 (D-E) were subjected to adipogenic differentiation and analyzed for expression of characteristic markers of adipocytes by RT-qPCR (A, C-E) and Western blot assay (B). \*  $P < .05$ , \*\*  $P < .01$ . A, mRNA expression of *PPAR $\gamma$ 2*, *FABP4*, *LPL*, *ADIPOQ*, and *CEBP $\alpha$* . Data are expressed as fold change relative to both the housekeeping gene and Standard condition.  $n = 8$ , Wilcoxon test. B, *PPAR $\gamma$ 2* and  $\beta$ -ACTIN loading control protein expression.  $n = 1$ . C, mRNA expression of characteristic markers of beige adipocytes (*UCP1*, *CIDEA*, and *PGC1 $\alpha$* ).  $n = 8$ , Wilcoxon. Data are expressed as fold change relative to both the housekeeping gene and Standard condition. D, mRNA expression of whole types of adipocyte markers (*PPAR $\gamma$ 2*, *FABP4*, *LPL*, and *ADIPOQ*) or (E) specific to beige adipocytes (*UCP1*, *CIDEA*, and *PGC1 $\alpha$* ).  $n = 2$ . Data are expressed as fold change relative to both the housekeeping gene and EGM2 P0 condition. EGM2, endothelial cell growth medium 2; hASCs, human adipose-derived stem/stromal cells

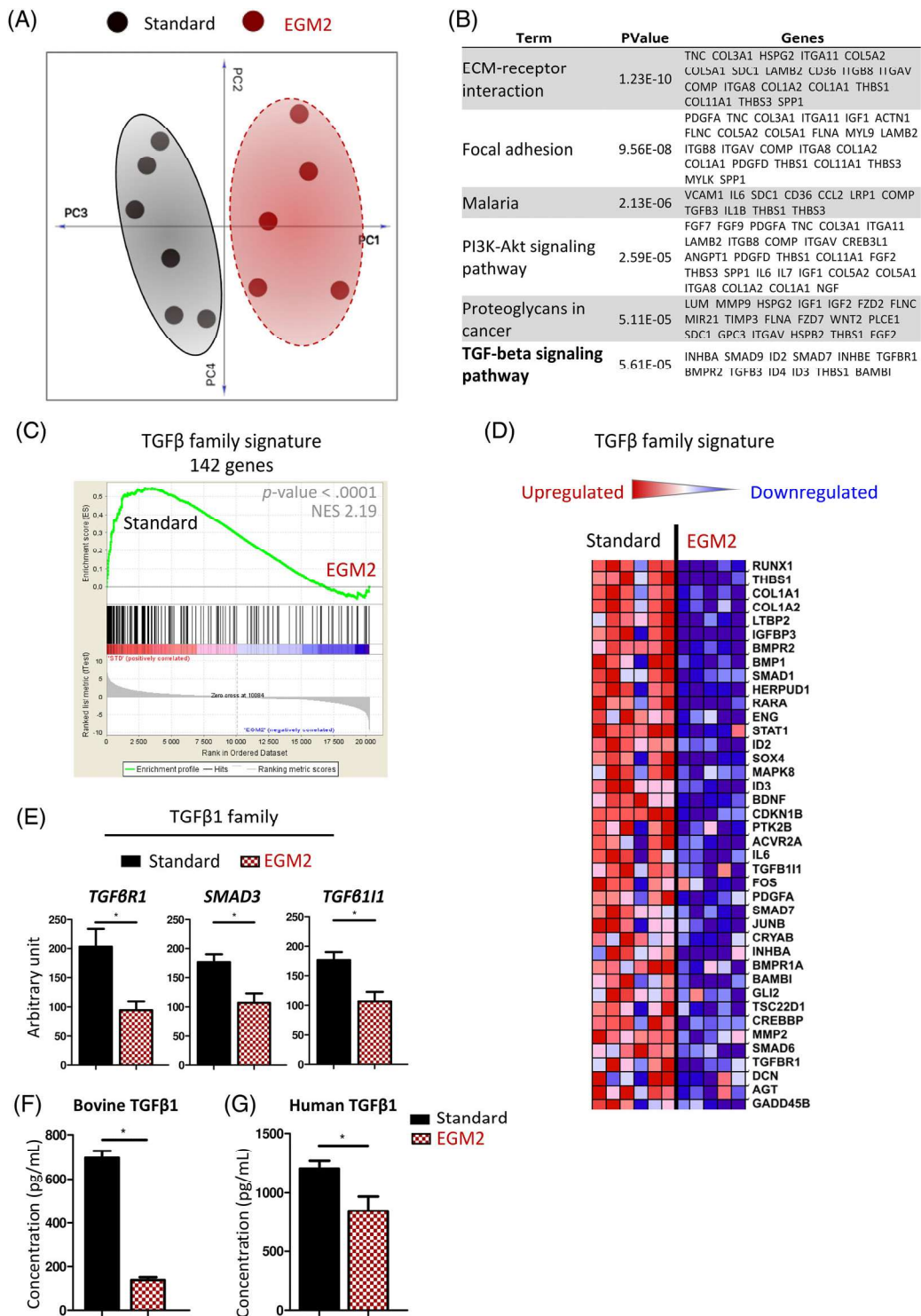


**FIGURE 3** TGFβ1 as a hallmark of Standard-hASCs. A-G, Standard-hASCs (black, n = 6) and EGM2-hASCs (red, n = 5) were analyzed by high throughput transcriptomic studies (A-E), and TGFβ1 in media (F) or supernatant (G) was evaluated. A, Analysis of four principal components for both types of hASCs. B, Significant gene ontology terms of pathway analysis for Standard-hASCs according to the corresponding P-value. C, Heat map representing the 40 top-expressed TGFβ-related genes overexpressed in Standard-hASCs compared with EGM2-hASCs. D, gene set enrichment analysis for TGFβ family signature in Standard-hASCs and EGM2-hASCs. Results were statistically significant according to FWER P-value depicted on the panel. E, mRNA expression of representative markers of the TGFβ1 pathway (*TGFβ1*, *SMAD3*, and *TGFβR1*) obtained from microarray studies. Wilcoxon test, \*  $P < .05$ . F, Bovine TGFβ1 concentration in Standard (black) and EGM2 (red) medium analyzed by sandwich enzyme linked immunosorbent assay (ELISA). n = 4, Mann-Whitney test, \*  $P < .05$ . G, Human TGFβ1 concentration in the supernatant of both hASCs types analyzed by sandwich ELISA. Data are expressed as fold change of level relative to Standard condition. n = 5, Mann-Whitney test, \*  $P < .05$ . EGM2, endothelial cell growth medium 2; SMAD, small mother of decapentaplegic homolog; hASCs, human adipose-derived stem/stromal cells; TGFβ1, transforming growth factor β1



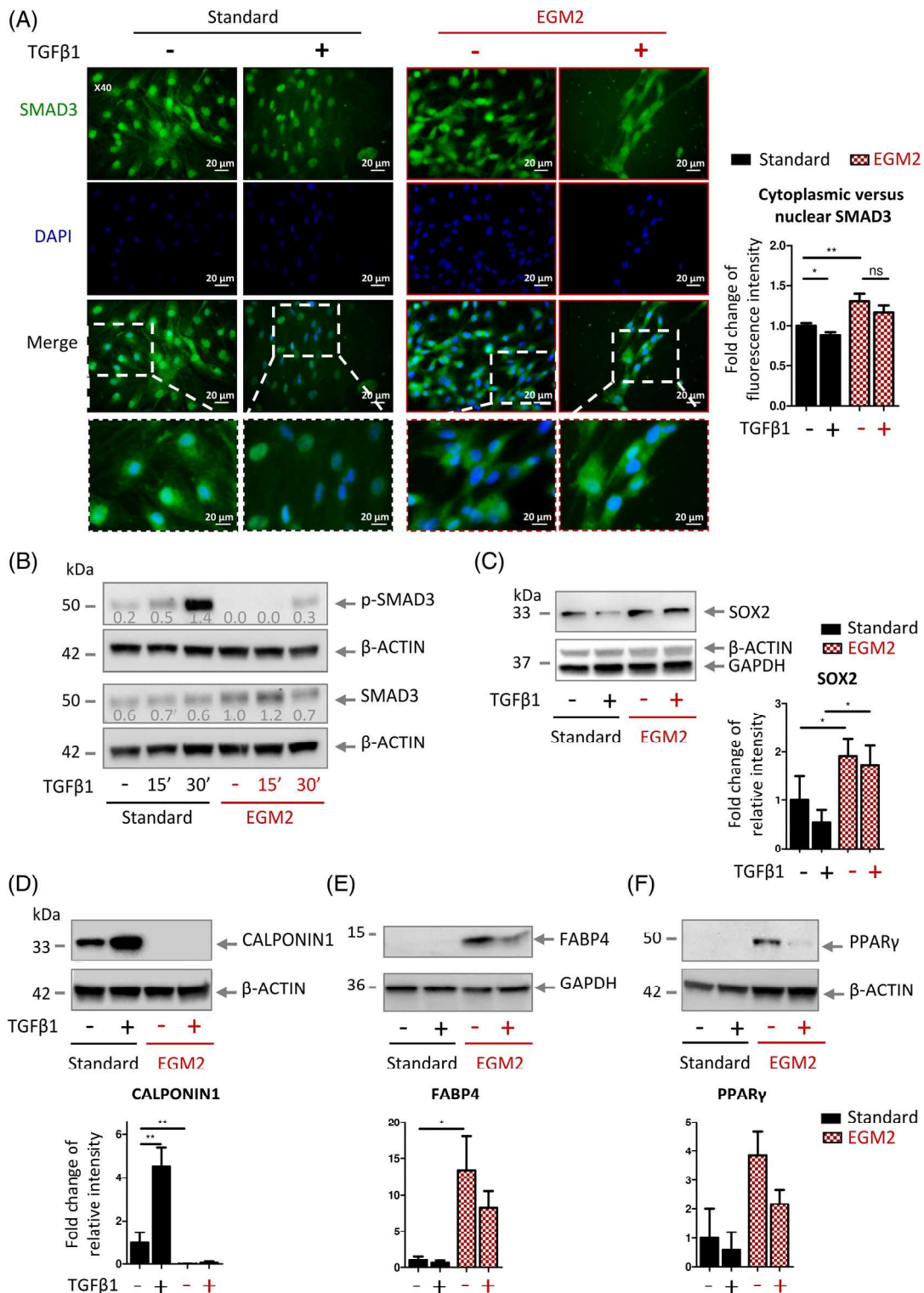


**FIGURE 4** Effect of TGFβ1 in Standard- and EGM2-hASCs. A-F, Standard-hASCs (black) and EGM2-hASCs (red) were treated (+) or not (–) with 10 ng/mL recombinant hTGFβ1 and analyzed by immunofluorescence (A) and Western blot assay (B–F). \*  $P < .05$ , \*\*  $P < .01$ . A, SMAD3 protein staining (green) in hASCs treated or not for 3 days. Nuclei were stained with DAPI. Images are representative of six independent experiments. Photonic microscopy. Scale bar = 20 μm, magnification = 40×. Mann-Whitney test. B, phospho-SMAD3 (Ser423/425) and total SMAD3 protein levels in hASCs treated or not for 15 or 30 minutes. β-ACTIN was a loading control.  $n = 4$ . C–F, SOX2 (C), CALPONIN1 (D), FABP4 (E), and PPARγ (F) protein levels in hASCs treated or not for 3 days. β-ACTIN or GAPDH was a loading control. Data were quantified according to band intensity normalized to the corresponding β-ACTIN band and expressed as fold change relative to Standard untreated condition. At least  $n = 4$ , Mann-Whitney test. EGM2, endothelial cell growth medium 2; hASCs, human adipose-derived stem/stromal cells; SMAD, small mother of decapentaplegic homolog; TGFβ1, transforming growth factor β1

analysis of mRNAs isolated from Standard-hASCs and EGM2-hASCs. We found a significant enrichment of GO terms associated with ECM-receptor interaction, focal adhesion, malaria, PI3K-Akt signaling, proteoglycans in cancer, and TGFβ-signaling pathway in Standard-hASCs compared with EGM2-hASCs (Figure 3B). These upregulated

pathways are known to be related to TGFβ signaling pathways. Therefore, we thought that TGFβ pathways might be altering the immaturity and multipotential of Standard-hASCs.

Following GSEA, we confirmed that mRNAs associated with TGFβ pathways were greatly upregulated in Standard-hASCs compared with

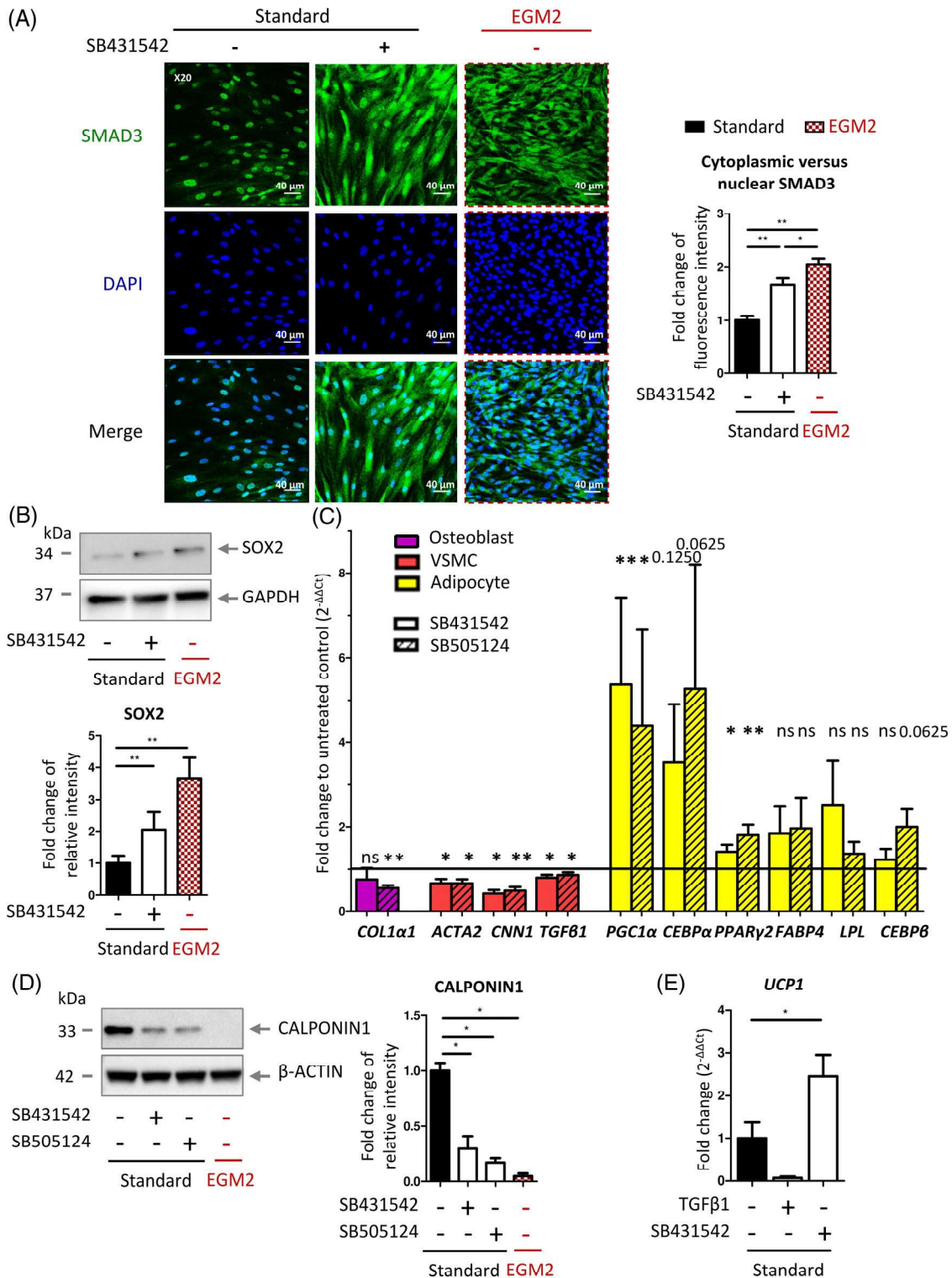


FIGURE 5 Legend on next page.

EGM2-hASCs (Figure 3C). Of note, transcriptomic analysis displayed on a heatmap showed an upregulation of the 40 most-expressed genes associated with TGF $\beta$  pathways, including TGF $\beta$ 1-inducible *TGF $\beta$ 111* and *TGF $\beta$ R1*, in Standard-hASCs vs EGM2-hASCs (Figure 3D). We next analyzed the TGF $\beta$ 1-associated mRNA contents. Consistently, we found that *TGF $\beta$ R1*, *SMAD3*, and *TGF $\beta$ 111* mRNA levels were increased by at least 1.25-fold in Standard-hASCs vs EGM2-hASCs (Figure 3E). This observation was supported by the finding of a fivefold higher content of bovine TGF $\beta$ 1 protein in standard medium than EGM2 medium. Also, Standard-hASCs secreted significantly more TGF $\beta$ 1 than did EGM2-hASCs (Figure 3F). Altogether, these results emphasized the increased activity of the TGF $\beta$ 1 pathway in Standard-hASCs.

To assess the actual implication of the TGF $\beta$ 1 pathway, we examined SMAD3 protein expression but also the cellular localization and phosphorylation of SMAD3 in Standard-hASCs and EGM2-hASCs. We found a pronounced SMAD3 nuclear staining in Standard-hASCs, with only a diffuse SMAD3 signal pattern detected in the cytoplasm of EGM2-hASCs (Figure 4A). The fluorescence intensity of SMAD3 in the cytoplasm, compared with the nucleus, was higher by about 25% in EGM2-hASCs than in Standard hASCs, which suggested lower TGF $\beta$ 1 activity in EGM2-hASCs (Figure 4A). This finding strongly suggested that the TGF $\beta$ 1 pathway activity was enhanced in Standard-hASCs compared with EGM2-hASCs. Subsequently, we analyzed the capacity of Standard-hASCs and EGM2-hASCs to respond to human recombinant TGF $\beta$ 1 (hrTGF $\beta$ 1) in vitro. All nuclei of Standard-hASCs contained SMAD3 after 3 days of stimulation with hrTGF $\beta$ 1, whereas in EGM2-hASCs, we did not detect nuclear SMAD3 (Figure 4A). Consistently, the content of phosphorylated-SMAD3 at Ser423-425, relative to whole SMAD3 protein content, was intensively increased in Standard-hASCs compared with EGM2-hASCs. Of note, this was observed with or without hrTGF $\beta$ 1 stimulation, which strengthens the former analysis suggesting the presence of activated SMAD3 in the nucleus of Standard-hASCs (Figure 4B).

Remarkably, the expression of SOX2 protein was not affected by hrTGF $\beta$ 1 stimulation in EGM2-hASCs, which suggests that EGM2-hASCs could retain their immaturity even upon TGF $\beta$ 1 stimulation (Figure 4C). Likewise, the level of the VSMC-associated protein

CALPONIN1 was strongly augmented in Standard-hASCs, but EGM2-hASCs did not express CALPONIN1 (Figure 4D). Also, hrTGF $\beta$ 1 stimulation in Standard-hASCs induced an increase in CALPONIN1 protein level by up to fourfold, with no effect in EGM2-hASCs (Figure 4D). Accordingly, *ACTA2* and *CNN1* VSMC lineage-associated mRNAs were upregulated by at least sixfold in Standard-hASCs compared with EGM2-hASCs (Figure S5a). Similarly, following hrTGF $\beta$ 1 stimulation, the mRNA levels of *ACTA2* and *CNN1* were increased by at least twofold in Standard-hASCs, but EGM2-hASCs were not significantly affected (Figure S5a). In parallel, we found an increase in mRNA levels associated with osteoblasts, including *DLX5*, by about 6-fold; *OSTERIX* about 80-fold; and *COL1 $\alpha$ 1* about 1.5-fold, in Standard-hASCs stimulated with hrTGF $\beta$ 1 than without hrTGF $\beta$ 1 (Figure S5b). Of note, the effect of hrTGF $\beta$ 1 on *DLX5* and *OSTERIX* mRNA expression was negligible in EGM2-hASCs, yet *COL1 $\alpha$ 1* mRNA level was significantly increased in EGM2-hASCs with than without hrTGF $\beta$ 1 stimulation (Figure S5b). In contrast, *FABP4* protein, a landmark of adipocytes, was expressed in EGM2-hASCs, but its expression was virtually absent in Standard-hASCs (Figure 4E). Similar results were found with PPAR $\gamma$  (Figure 4F). Here, stimulation of Standard-hASCs or EGM2-hASCs with hrTGF $\beta$ 1 tended to alter the protein expression of both *FABP4* and PPAR $\gamma$  (Figure 4E,F). Accordingly, adipogenic lineage-associated mRNAs including *FABP4* and *LPL* were upregulated about 10- and 2-fold, respectively, in EGM2-hASCs compared with Standard-hASCs, which strengthens our previous findings suggesting an enhanced adipogenic potential of EGM2-hASCs (Figure S5c). Upon hrTGF $\beta$ 1 stimulation, *FABP4* and *LPL* mRNA levels were significantly decreased by at least twofold in both Standard-hASCs and EGM2-hASCs (Figure S5c), so the adipogenic potential of hASCs can be affected by TGF $\beta$ 1.

TGF $\beta$ 1 mRNA level was higher in Standard-hASCs than EGM2-hASCs (Figure S5d). Of note, EGM2-hASCs stimulated with hrTGF $\beta$ 1 exhibited a significant increase in TGF $\beta$ 1 mRNA level, which suggests a TGF $\beta$ 1 amplification loop (Figure S5d). Hence, these data confirmed that Standard-hASCs were sensitized to TGF $\beta$ 1 signaling and that the addition of hrTGF $\beta$ 1 increased the Standard-hASC commitment into osteoblast, chondroblast, and VSMC lineages at the expense of adipocyte lineage.

**FIGURE 5** Inhibition of TGF $\beta$ 1 effects on Standard-hASCs. A-E, Standard-hASCs (black) and EGM2-hASCs (red) were treated (+) or not (–) with 1  $\mu$ M TGF $\beta$ 1 receptor inhibitor for 3 days (SB431542 or SB505124, as specified in figure), and analyzed by immunofluorescence (A), Western blot analysis (B, D) or RT-qPCR (C, E) before (A-D) or after (E) adipogenic differentiation. \*  $P < .05$ , \*\*  $P < .01$ . A, SMAD3 protein staining (green) in hASCs. Nuclei were stained with DAPI. Images are representative of six independent experiments. Confocal microscopy. Scale bar = 40  $\mu$ m, magnification = 20 $\times$ . Mann-Whitney test. B, SOX2 protein levels. GAPDH was a loading control. Data were quantified according to band intensity normalized to the corresponding GAPDH band and expressed as fold change relative to Standard untreated condition.  $n = 8$ , Wilcoxon test. C, mRNA expression of osteoblast (*COL1 $\alpha$ 1*), VSMC (*ACTA2*, *CNN1*, and *TGF $\beta$ 1*), and adipocyte (*PGC1 $\alpha$* , *CEBP $\alpha$* , *PPAR $\gamma$ 2*, *FABP4*, *LPL*, and *CEBP $\beta$* ) characteristic markers in Standard-hASCs. Data are expressed as fold change relative to both the housekeeping gene and untreated condition.  $n = 7$ , Wilcoxon test. D, CALPONIN1 protein level.  $\beta$ -ACTIN was a loading control. Data were quantified according to band intensity normalized to the corresponding  $\beta$ -ACTIN band and expressed as fold change relative to Standard untreated condition.  $n = 3$ , Mann-Whitney test. E, mRNA expression of *UCP1* in Standard-hASCs treated (+) or not (–) with 10 ng/mL recombinant hrTGF $\beta$ 1 or 1  $\mu$ M TGF $\beta$ 1 receptor inhibitor SB431542 for 3 days before 11 days of adipogenic differentiation and overnight forskolin stimulation. Data are expressed as fold change relative to both the housekeeping gene and untreated condition.  $n = 6$ , Mann-Whitney test. EGM2, endothelial cell growth medium 2; hASCs, human adipose-derived stem/stromal cells; SMAD, small mother of decapentaplegic homolog; TGF $\beta$ 1, transforming growth factor  $\beta$ 1



### 3.5 | Blockade of TGFβ1 pathway restores immaturity and adipogenesis potential of Standard-hASCs

To strengthen the hypothesis that TGFβ1 influenced the fate of Standard-hASCs, we evaluated the effect of inhibitors of the TGFβ1 pathway on the adipogenic potential. To this end, we used two pharmacological inhibitors of TGFβ1R, SB431542, and SB505124. The addition of SB431542 was associated with a cytoplasmic SMAD3 localization in Standard-hASCs, to an extent comparable to that observed in EGM2-hASCs (Figure 5A). Of note, SOX2 protein content was increased in Standard-hASCs in the presence of SB431542, which suggests a reinstatement of cell immaturity features (Figure 5B). We next sought to determine whether TGFβ1R inhibition might restore the adipogenic potential in Standard-hASCs. In Standard-hASCs, both SB431542 and SB505124 decreased the mRNA level of osteoblast lineage-associated *COL1α1* as well as the levels of VSMC lineage-associated *ACTA2*, *CNN1*, and *TGFβ1*. Both SB431542 and SB505124 greatly enhanced levels of adipocyte lineage-associated mRNAs, including *PGC1α*, *CEBPα*, *PPARγ2*, *FABP4*, *LPL*, and *CEBPβ*, in Standard-hASCs (Figure 5C). Remarkably, SB431542 and SB505124 significantly reduced CALPONIN1 protein content in Standard-hASCs to a comparable level to that observed in EGM2-hASCs (Figure 5D). Importantly, SB431542 improved the Standard-hASC ability to differentiate into beige adipocytes upon forskolin stimulation, as assessed by the upregulation of *UCP1* compared with controls (Figure 5E).

## 4 | DISCUSSION

Human ASCs exhibit functional characteristics of interest in cell therapy and regenerative medicine. Here, we studied the effect of culture conditions on ASC characteristics. We compared a medium with low TGFβ1 content, as in EGM2, to one with higher TGFβ1 content, as in standard conditions. It appeared that low TGFβ1 content was associated with a certain immaturity of primary hASCs during in vitro expansion, with a higher concentration of TGFβ1-primed hASCs toward osteoblast, chondroblast and VSMC lineages. Importantly, this priming was associated with reduced adipogenic potential (Figure S6).

In dealing with adult multipotent cells in a cell therapy perspective, it is crucial to keep the differentiation potential of these cells, a feature linked to cell immaturity. The immature state of cells is evaluated by both the expression of specific pluripotency-associated genes and the downregulation of specific lineage markers. We observed that EGM2-hASCs exhibited increased SOX2, OCT4, and NANOG protein levels compared with Standard-hASCs. The expression of those “stemness markers” revealed the enhanced immature state of hASCs under EGM2 conditions vs standard conditions.<sup>28-32</sup> This observation underlies the strong ability of EGM2-hASCs to differentiate into osteoblast, chondroblast, and adipocytes. The differentiation process corresponds to sequential acquisition of specific features and markers of the mature cell type.<sup>33,34</sup> This process is associated with the loss of

the proliferative abilities of the cells.<sup>35</sup> Here, we found low mRNA levels of osteoblast, chondroblast, and VSMC-lineage markers in proliferative EGM2-hASCs compared with Standard-hASCs. This finding suggests that EGM2-hASCs were less engaged toward those lineages, being in a more immature state. We previously found similar results with EGM2-BM-MSCs, even if we did not identify in this study TGFβ1 as a regulator of immaturity and differentiation abilities.<sup>36</sup> Nevertheless, despite being more immature, both EGM2-hASCs and EGM2-BM-MSCs still showed the expression, albeit at a low level, of lineage markers. This observation agrees with the Dov Zipori hypothesis and the results of Pierre Charbord's team on human BM-MSCs.<sup>37</sup> In clonal and non-clonal high throughput transcriptomic studies, BM-MSCs expressed osteoblast, chondroblast, VSMC, and adipocyte lineage markers at a basal state.<sup>38</sup> Differentiation of BM-MSCs induced an increase of the intended genomic program and downregulation of lineage-unspecific genes.<sup>38</sup> Other wide-range biocomputing studies, gathering transcriptomic data from several published reports and using MSCs from different tissue origins, also showed this lineage priming.<sup>39</sup> Our study highlighted that the TGFβ1 contained in the serum of standard medium induced the expression of osteoblast, chondroblast, and VSMC lineage markers in hASCs. In the literature, BM-MSCs were mostly expanded in standard conditions. Thus, the expression at a low level of lineage markers detected in BM-MSCs could result from TGFβ1 activity. In order to determine whether immaturity is associated to constitutive low-grade expression of lineage markers, or to bias from culture conditions, the expression of lineage markers could be evaluated in native BM-MSCs and hASCs.

Although EGM2-hASCs appeared more immature than Standard-hASCs, overexpression of mRNAs and proteins related to the adipocyte lineage suggested that EGM2-hASCs were committed toward an adipocyte lineage. Given the significantly higher proliferation capacities (Figure S1d) and immaturity marks of EGM2-hASCs than Standard-hASCs, we could wonder whether EGM2-hASCs were less engaged toward an adipocyte lineage than Standard-hASCs were toward osteoblast, chondroblast, and VSMC lineages. Because the stiffness of plastic culture flasks can decrease the ability of BM-MSCs to differentiate into mature adipocytes, we similarly could suspect that EGM2-hASCs were restrained in their adipogenic commitment.<sup>40</sup> In our study, functional experiments demonstrated the deleterious effects of TGFβ1 on adipogenesis. Indeed, EGM2 contained  $137.5 \pm 12.6$  pg/mL of TGFβ1 protein (Figure 3F), fivefold less TGFβ1 than with standard medium. Hence, this TGFβ1 could be sufficient to impede the strong priming of EGM2-hASCs toward adipogenesis at baseline. Finally, the immature state of EGM2-hASCs maintained a potential to differentiate into osteoblasts and chondroblasts, to the same extent as Standard-hASCs (Figures 1A and S1A). Altogether, these observations suggested that EGM2-hASCs could be more immature cells rather than committed to an adipocyte lineage.

Our data also confirmed that Standard-hASCs remained sensitive to TGFβ1 signaling and that further addition of hrTGFβ1 increased the commitment into osteoblast, chondroblast, and VSMC lineages at the expense of adipogenesis. The role of TGFβ1 in osteoblast, chondroblast, and VSMC lineages was previously evaluated in different



cell models.<sup>41-46</sup> Our data confirmed TGF $\beta$ 1 as a major factor with broad influence on the fate of primary hASCs in their plasticity. Also, we showed that EGM2-hASCs were not responsive to TGF $\beta$ 1 for osteoblast, chondroblast, and VSMC lineages but were sensitive for adipocyte priming. Recently, the SVF of mouse and human adipose tissues were analyzed by single-cell RNA-seq and functional experiments.<sup>47</sup> This work demonstrated that the low adipogenic capabilities of DPP4<sup>+</sup> cells, compared with ICAM1<sup>+</sup> cells, were due to differential TGF $\beta$ 1 sensitivity. Our work confirmed that hASCs were heterogeneously sensitive to TGF $\beta$ 1 and suggested that EGM2 medium maintained their adipogenic capacities.

Here, we demonstrated the negative effect of TGF $\beta$ 1 on adipogenic differentiation of hASCs, particularly on beige adipocyte potential. The ability of hASCs to differentiate *in vitro* in beige adipocytes is well described.<sup>48-50</sup> However, there was room for improvement of this potential by adapting culture conditions, which we achieved by using EGM2 medium. Nevertheless, functional experiments such as mitochondrial respiration measurements would be needed to complete the demonstration of the beige phenotype in further studies. Of note, we recently published that EGM2 conditions enabled the formation and maintenance of highly vascularized 3D spheroids containing both unilocular and multilocular adipocytes.<sup>51</sup> Importantly, we revealed the persistence of human adipocytes after *in vivo* transplantation in mice, together with chimeric human/murine vessels.<sup>51</sup>

Although both being a member of the TGF $\beta$  superfamily, BMP7 and TGF $\beta$ 1 have opposite effect, BMP7 being inducer of beige/brown adipogenesis in mice and human.<sup>52,53</sup> Similarly, BMP4 is essential for adipogenesis, even if its ability to promote white-to-brown or brown-to-white adipocyte conversion remains discussed.<sup>54,55</sup> It is noteworthy that BMPs signal through specific receptors and SMAD-1, SMAD-5, SMAD-8, which differs from those involved in TGF $\beta$ 1 signaling pathway. Even if BMPs and TGF $\beta$ 1 belong to the TGF $\beta$  superfamily, they might bear distinct effects on hASC differentiation.

We next showed that the TGF $\beta$ 1 effects on Standard-hASCs could be overturned by using pharmacological inhibitors of TGF $\beta$ R, promoting immaturity and expression of adipogenic lineage biomarkers. Furthermore, blocking the TGF $\beta$ 1 pathway increased beige adipocyte potential. This finding agrees with the need for SB431542 in EGM2 medium to trigger strong beige adipocyte differentiation from induced pluripotent stem cells.<sup>56</sup> In addition, SMAD3-null mice exhibited browning of their white adipose tissue with the appearance of beige adipocytes among white adipocytes.<sup>8,57,58</sup> From a therapeutic point of view, browning of adipose tissue enhanced systemic insulin sensitivity and glucose tolerance in mice, and protected the animals against high-fat diet-induced obesity and diabetes. Similar results were recently obtained for TGF $\beta$ R1-deficient mice.<sup>59</sup> Conversely, *in vivo* intraperitoneal injection of TGF $\beta$ 1 downregulated beige adipocyte markers, including UCP1, in white adipose tissue.<sup>8</sup> Finally, beige adipocytes obtained from human adipose-tissue explants cultured in EGM2 conditions could improve the glucose metabolism of obese NSG mice.<sup>7</sup>

Therefore, blockade of the TGF $\beta$ 1 pathway or utilization of EGM2 medium to expand primary hASCs could help retain immature

features of hASCs *in vitro* and strong beige adipocyte differentiation abilities. It is noteworthy that EGM2 medium contains EGF, FGF2, IGF1, VEGF, ascorbic acid, heparin, and hydrocortisone, which could influence immaturity and adipogenic potential of hASCs. For instance, Hafner et al studied the impact of each factor on adipogenesis from induced pluripotent stem cells.<sup>56</sup> They showed that hydrocortisone, ascorbic acid, and EGF were required for brown adipocyte differentiation. The positive effect of EGF on adipocyte differentiation was confirmed in a mouse model.<sup>60</sup> In addition, even if immaturity was not studied, Suga et al described a positive effect of FGF2 on proliferative abilities of EGM2-hASCs.<sup>61</sup> These studies confirmed that media composition was crucial to improve and control the potentialities of hASCs.

In the clinic, beige adipocyte differentiation abilities of hASCs could be valorized to combat obesity and diabetes. Considering the numerous clinical trials using hMSCs or hASCs to treat a large panel of degenerative diseases or injuries, there is a need to optimize culture conditions to obtain high cell yields.

## 5 | CONCLUSION

Here, we showed that medium containing TGF $\beta$ 1 induced differentiation toward osteoblast, chondroblast, and VSMC lineages of primary hASCs and reduced adipogenic potential. With reduced TGF $\beta$ 1 content, EGM2 maintained the high immaturity features of hASCs, allowing to exploit their strong white and beige adipogenic potential. Hence, we encourage paying particular attention to TGF $\beta$ 1 content for MSC cultures in research as well as for clinical objectives.

## ACKNOWLEDGMENTS

The authors acknowledge Yannick Jeanson and Noémie Juin for their technical expertise. This work was supported by the Etablissement Français du Sang Scientific Council (APR 2014). HL received funding from the French Research and Educational Ministry at Paul Sabatier University and the Etablissement Français du Sang. AN received funding from the Japanese Society for the Promotion of Science (JSPS), Young B KAKENHI (Grant No. 17K15729).

## CONFLICT OF INTEREST

The authors declared no potential conflicts of interest.

## AUTHOR CONTRIBUTIONS

H.L., F.G.: conception and design, collection and/or assembly of data, data analysis and interpretation, manuscript writing; F.D.: conception and design, data analysis and interpretation, manuscript editing; J.G. D.: collection and/or assembly and data analysis; L.F.: data analysis; A. C., J.C.P., L.C., L.S.: conception, manuscript editing. A.N., N.S.: data analysis, manuscript editing; C.B.: provision of human material. All authors: final approval of the manuscript.

## DATA AVAILABILITY STATEMENT

Gene signatures and raw data are accessible in the Gene Expression Omnibus (GEO) repository platform (GSE136778).

## ORCID

Hélène Leménager  <https://orcid.org/0000-0001-8829-3386>

## REFERENCES

- Pittenger MF, Mackay AM, Beck SC, et al. Multilineage potential of adult human mesenchymal stem cells. *Science*. 1999;284:143-147.
- Bianco P, Cao X, Frenette PS, et al. The meaning, the sense and the significance: translating the science of mesenchymal stem cells into medicine. *Nat Med*. 2013;19:35-42.
- Naji A, Eitoku M, Favier B, et al. Biological functions of mesenchymal stem cells and clinical implications. *Cell Mol Life Sci*. 2019;76:3323-3348.
- Zuk PA, Zhu M, Ashjian P, et al. Human adipose tissue is a source of multipotent stem cells. *Mol Biol Cell*. 2002;13:4279-4295.
- Finlin BS, Memetimin H, Confides AL, et al. Human adipose beiging in response to cold and mirabegron. *JCI Insight*. 2018;3:e121510.
- Cousin B, Cinti S, Morroni M, et al. Occurrence of brown adipocytes in rat white adipose tissue: molecular and morphological characterization. *J Cell Sci*. 1992;103(Pt 4):931-942.
- Min SY, Kady J, Nam M, et al. Human "brite/beige" adipocytes develop from capillary networks, and their implantation improves metabolic homeostasis in mice. *Nat Med*. 2016;22:312-318.
- Yadav H, Quijano C, Kamaraju AK, et al. Protection from obesity and diabetes by blockade of TGF-β/Smad3 signaling. *Cell Metab*. 2011;14:67-79.
- Rosenwald M, Perdikari A, Rüllicke T, et al. Bi-directional interconversion of brite and white adipocytes. *Nat Cell Biol*. 2013;15:659-667.
- Tang W, Zeve D, Suh JM, et al. White fat progenitor cells reside in the adipose vasculature. *Science*. 2008;322:583-586.
- Crisan M, Yap S, Casteilla L, et al. A perivascular origin for mesenchymal stem cells in multiple human organs. *Cell Stem Cell*. 2008;3:301-313.
- Long JZ, Svensson KJ, Tsai L, et al. A smooth muscle-like origin for beige adipocytes. *Cell Metab*. 2014;19:810-820.
- Tran K-V, Gealekman O, Frontini A, et al. The vascular endothelium of the adipose tissue gives rise to both white and brown fat cells. *Cell Metab*. 2012;15:222-229.
- Oida T, Weiner HL. Depletion of TGF-β from fetal bovine serum. *J Immunol Methods*. 2010;362:195-198.
- Weiss A, Attisano L. The TGFβ superfamily signaling pathway. *Wiley Interdiscip Rev Dev Biol*. 2013;2:47-63.
- Shi M, Zhu J, Wang R, et al. Latent TGF-β structure and activation. *Nature*. 2011;474:343-349.
- Brown PD, Wakefield LM, Levinson AD, et al. Physicochemical activation of recombinant latent transforming growth factor-beta's 1, 2, and 3. *Growth Factors*. 1990;3:35-43.
- Lyons RM, Keski-Oja J, Moses HL. Proteolytic activation of latent transforming growth factor-beta from fibroblast-conditioned medium. *J Cell Biol*. 1988;106:1659-1665.
- Khalil N. TGF-beta: from latent to active. *Microbes Infect*. 1999;1:1255-1263.
- Massagué J. TGFβ signalling in context. *Nat Rev Mol Cell Biol*. 2012;13:616-630.
- Gronthos S, Zannettino ACW, Hay SJ, et al. Molecular and cellular characterisation of highly purified stromal stem cells derived from human bone marrow. *J Cell Sci*. 2003;116:1827-1835.
- Subramanian A, Tamayo P, Mootha VK, et al. Gene set enrichment analysis: a knowledge-based approach for interpreting genome-wide expression profiles. *Proc Natl Acad Sci U S A*. 2005;102:15545-15550.
- Mootha VK, Lindgren CM, Eriksson K-F, et al. PGC-1α-responsive genes involved in oxidative phosphorylation are coordinately down-regulated in human diabetes. *Nat Genet*. 2003;34:267-273.
- Huang DW, Sherman BT, Lempicki RA. Systematic and integrative analysis of large gene lists using DAVID bioinformatics resources. *Nat Protoc*. 2009;4:44-57.
- Huang DW, Sherman BT, Lempicki RA. Bioinformatics enrichment tools: paths toward the comprehensive functional analysis of large gene lists. *Nucleic Acids Res*. 2009;37:1-13.
- Rodda DJ, Chew J-L, Lim L-H, et al. Transcriptional regulation of nanog by OCT4 and SOX2. *J Biol Chem*. 2005;280:24731-24737.
- Merlin J, Sato M, Nowell C, et al. The PPARγ agonist rosiglitazone promotes the induction of brite adipocytes, increasing β-adrenoceptor-mediated mitochondrial function and glucose uptake. *Cell Signal*. 2018;42:54-66.
- Takahashi K, Tanabe K, Ohnuki M, et al. Induction of pluripotent stem cells from adult human fibroblasts by defined factors. *Cell*. 2007;131:861-872.
- Arnold K, Sarkar A, Yram MA, et al. Sox2(+) adult stem and progenitor cells are important for tissue regeneration and survival of mice. *Cell Stem Cell*. 2011;9:317-329.
- Tompkins DH, Besnard V, Lange AW, et al. Sox2 is required for maintenance and differentiation of bronchiolar Clara, ciliated, and goblet cells. *PLoS One*. 2009;4:e8248.
- Lai Y-S, Chang C-W, Pawlik KM, et al. SRY (sex determining region Y)-box2 (Sox2)/poly ADP-ribose polymerase 1 (Parp1) complexes regulate pluripotency. *Proc Natl Acad Sci U S A*. 2012;109:3772-3777.
- Wuebben EL, Rizzino A. The dark side of SOX2: cancer - a comprehensive overview. *Oncotarget*. 2017;8:44917-44943.
- Uccelli A, Moretta L, Pistoia V. Mesenchymal stem cells in health and disease. *Nat Rev Immunol*. 2008;8:726-736.
- Laurenti E, Göttgens B. From haematopoietic stem cells to complex differentiation landscapes. *Nature*. 2018;553:418-426.
- Ruijtenberg S, van den Heuvel S. Coordinating cell proliferation and differentiation: antagonism between cell cycle regulators and cell type-specific gene expression. *Cell Cycle*. 2016;15:196-212.
- Bouacida A, Rosset P, Trichet V, et al. Pericyte-like progenitors show high immaturity and engraftment potential as compared with mesenchymal stem cells. *PLoS One*. 2012;7:e48648.
- Zipori D. The nature of stem cells: state rather than entity. *Nat Rev Genet*. 2004;5:873-878.
- Delorme B, Ringe J, Pontikoglou C, et al. Specific lineage-priming of bone marrow mesenchymal stem cells provides the molecular framework for their plasticity. *STEM CELLS*. 2009;27:1142-1151.
- Roson-Burgo B, Sanchez-Guijo F, Del Cañizo C, et al. Insights into the human mesenchymal stromal/stem cell identity through integrative transcriptomic profiling. *BMC Genomics*. 2016;17:944.
- Talele NP, Fradette J, Davies JE, et al. Expression of α-smooth muscle Actin determines the fate of mesenchymal stromal cells. *Stem Cell Rep*. 2015;4:1016-1030.
- Xia W, Jin Y-Q, Kretlow JD, et al. Adenoviral transduction of hTGF-beta1 enhances the chondrogenesis of bone marrow derived stromal cells. *Biotechnol Lett*. 2009;31:639-646.
- Mehlhorn AT, Niemeyer P, Kaschte K, et al. Differential effects of BMP-2 and TGF-beta1 on chondrogenic differentiation of adipose derived stem cells. *Cell Prolif*. 2007;40:809-823.
- Zhao L, Jiang S, Hantash BM. Transforming growth factor beta1 induces osteogenic differentiation of murine bone marrow stromal cells. *Tissue Eng Part A*. 2010;16:725-733.
- Maeda S, Hayashi M, Komiya S, et al. Endogenous TGF-beta signaling suppresses maturation of osteoblastic mesenchymal cells. *EMBO J*. 2004;23:552-563.
- Hautmann MB, Madsen CS, Owens GK. A transforming growth factor beta (TGFβ) control element drives TGFβ-induced stimulation of smooth muscle alpha-Actin gene expression in concert with two CArG elements. *J Biol Chem*. 1997;272:10948-10956.
- Yang H, Zhang L, Weakley SM, et al. Transforming growth factor-beta increases the expression of vascular smooth muscle cell markers in human multi-lineage progenitor cells. *Med Sci Monit*. 2011;17:BR55-BR61.

47. Merrick D, Sakers A, Irgebay Z, et al. Identification of a mesenchymal progenitor cell hierarchy in adipose tissue. *Science*. 2019;364: eaav2501.
48. Khanh VC, Zulkifli AF, Tokunaga C, et al. Aging impairs beige adipocyte differentiation of mesenchymal stem cells via the reduced expression of Sirtuin 1. *Biochem Biophys Res Commun*. 2018;500:682-690.
49. Bartesaghi S, Hallen S, Huang L, et al. Thermogenic activity of UCP1 in human white fat-derived beige adipocytes. *Mol Endocrinol*. 2015; 29:130-139.
50. Nyman E, Bartesaghi S, Melin Rydfalk R, et al. Systems biology reveals uncoupling beyond UCP1 in human white fat-derived beige adipocytes. *NPJ Syst Biol Appl*. 2017;3:29.
51. Muller S, Ader I, Creff J, et al. Human adipose stromal-vascular fraction self-organizes to form vascularized adipose tissue in 3D cultures. *Sci Rep*. 2019;9:7250.
52. Okla M, Ha J-H, Temel RE, et al. BMP7 drives human adipogenic stem cells into metabolically active beige adipocytes. *Lipids*. 2015;50: 111-120.
53. Tseng Y-H, Kokkotou E, Schulz TJ, et al. New role of bone morphogenetic protein 7 in brown adipogenesis and energy expenditure. *Nature*. 2008;454:1000-1004.
54. Elsen M, Raschke S, Tennagels N, et al. BMP4 and BMP7 induce the white-to-brown transition of primary human adipose stem cells. *Am J Physiol Cell Physiol*. 2014;306:C431-C440.
55. Modica S, Straub LG, Balaz M, et al. Bmp4 promotes a Brown to white-like adipocyte shift. *Cell Rep*. 2016;16:2243-2258.
56. Hafner A-L, Contet J, Ravaud C, et al. Brown-like adipose progenitors derived from human induced pluripotent stem cells: identification of critical pathways governing their adipogenic capacity. *Sci Rep*. 2016; 6:32490.
57. Tiano JP, Springer DA, Rane SG. SMAD3 negatively regulates serum irisin and skeletal muscle FNDC5 and peroxisome proliferator-activated receptor  $\gamma$  coactivator 1- $\alpha$  (PGC-1 $\alpha$ ) during exercise. *J Biol Chem*. 2015;290:11431.
58. McDonald ME, Li C, Bian H, et al. Myocardin-related transcription factor a regulates conversion of progenitors to beige adipocytes. *Cell*. 2015;160:105-118.
59. Wankhade UD, Lee J-H, Dagur PK, et al. TGF- $\beta$  receptor 1 regulates progenitors that promote browning of white fat. *Mol Metab*. 2018;16: 160-171.
60. Harrington M, Pond-Tor S, Boney CM. Role of epidermal growth factor and ErbB2 receptors in 3T3-L1 adipogenesis. *Obesity (Silver Spring)*. 2007;15:563-571.
61. Suga H, Shigeura T, Matsumoto D, et al. Rapid expansion of human adipose-derived stromal cells preserving multipotency. *Cytherapy*. 2007;9:738-745.

#### SUPPORTING INFORMATION

Additional supporting information may be found online in the Supporting Information section at the end of this article.

**How to cite this article:** Leménager H, Fiévet LMA, Guilloton F, et al. Cell immaturity and white/beige adipocyte potential of primary human adipose-derived stromal cells are restrained by culture-medium TGF $\beta$ 1. *Stem Cells*. 2020;38: 782-796. <https://doi.org/10.1002/stem.3164>